Altered brain morphology after focal radiation reveals impact of off-target effects: implications for white matter development and neurogenesis

Kiran G. Beera, Yu-Qing Li, Jun Dazai, James Stewart, Shannon Egan, Mashal Ahmed, C. Shun Wong, David A. Jaffray, and Brian J. Nieman

Mouse Imaging Centre, Hospital for Sick Children, Toronto, Ontario, Canada (K.G.B., J.D., S.E., M.A., B.J.N.); Department of Medical Biophysics, University of Toronto, Toronto, Ontario, Canada (K.G.B., C.S.W., D.A.J., B.J.N.); Department of Radiation Oncology, Sunnybrook Health Sciences Centre, Toronto, Ontario, Canada (Y.Q.L., C.S.W.); Institute of Biomaterials and Biomedical Engineering, University of Toronto, Toronto, Ontario, Canada (J.S., D.A.J.); Princess Margaret Cancer Centre, Radiation Medicine Program, Techna Institute, University Health Network, Toronto, Ontario, Canada (D.A.J.); Department of Physics, University of McGill, Montreal, Quebec, Canada (S.E.); Department of Biology, University of Waterloo, Waterloo, Ontario, Canada (M.A.); Department of Radiation Oncology, University of Toronto, Toronto, Ontario, Canada (C.S.W.); Ontario Institute for Cancer Research, Toronto, Ontario, Canada (B.J.N.)

Corresponding Author: Brian J. Nieman, Mouse Imaging Centre, Hospital for Sick Children, 25 Orde Street, Toronto, ON, Canada M5T 3H7 (brian.nieman@sickkids.ca).

Abstract

Background: Children with brain tumors treated with cranial radiation therapy (RT) often exhibit cognitive late effects, commonly associated with reduced white matter (WM) volume and decreased neurogenesis. The impact of radiation damage in particular regions or tissues on brain development as a whole has not been elucidated.

Methods: We delivered whole-brain or focal radiation (8 Gy single dose) to infant mice. Focal treatments targeted white matter (anterior commissure), neuronal (olfactory bulbs), or neurogenic (subventricular zone) regions. High-resolution ex vivo MRI was used to assess radiation-induced volume differences. Immunohistochemistry for myelin basic protein and doublecortin was performed to assess associated cellular changes within white matter and related to neurogenesis, respectively.

Results: Both whole-brain and focal RT in infancy resulted in volume deficits in young adulthood, with whole-brain RT resulting in the largest deficits. RT of the anterior commissure, surprisingly, showed no impact on its volume or on brain development as a whole. In contrast, RT of the olfactory bulbs resulted in off-target volume reduction in the anterior commissure and decreased subventricular zone neurogenesis. RT of the subventricular zone likewise produced volume deficits in both the olfactory bulbs and the anterior commissure. Similar off-target effects were found in the corpus callosum and parietal cortex.

Conclusions: Our results demonstrate that radiation damage locally can have important off-target consequences for brain development. These data suggest that WM may be less radiosensitive than volume change alone would indicate and have implications for region-sparing radiation treatments aimed at reducing cognitive late effects.

Key words

brain development | MRI | neurogenesis | radiation | white matter

Radiation therapy (RT) is a critical component of treatment for pediatric CNS tumors such as medulloblastoma. Depending on the tumor type, the current standard of care generally includes surgical resection of the tumor, followed by craniospinal RT and/or chemotherapy.[1] Children who receive RT frequently experience late toxicities, also known

Importance of the study

Previous literature has shown that radiation-induced cognitive deficits in survivors of pediatric brain tumors are associated with structural changes in the brain. In this study, we systematically target select substructures of the brain—including white matter, neuronal, and neurogenic tissues—using focal radiation in the infant mouse to assess the global developmental impact of localized radiation damage in these tissues. Results show that both white matter volume and neurogenesis can be significantly impacted by off-target effects after irradiation of other structures, highlighting the importance of ongoing development in the pediatric brain's response to radiation. Furthermore, it appears that white matter in fact exhibits little radiation-induced volume change when targeted in isolation. Successful adaptation of cranial radiation treatment and/or reduction of cognitive deficits in childhood cancer survivors will depend on understanding the distribution and mechanisms of off-target effects.

as late effects.[2] In the brain, these late effects may manifest as cognitive, behavioral, social, and/or hormonal deficits months to years after RT and are ultimately associated with lower socioeconomic status and poorer quality of life.[3,4] Significant reductions in total white matter (WM) volume after cranial RT have been observed in cancer survivors.[5,6] Underlying cellular changes resulting from radiation injury have been identified, primarily using rodent models, and include changes in neuronal architecture,[7] reduced oligodendrocyte and oligodendrocyte precursor cell populations,[8,9] and impaired neurogenesis.[10–12] Radiation-treated mice also exhibit changes in behavior and learning, including: altered locomotor activity; increased anxiety; transient changes in aggression; and impaired place learning, object recognition, and spatial memory.[13–16] Brain structure changes after RT in mice are likewise consistent with observations in human survivors.[17]

In the context of development, the overall impact of radiation damage to one brain region is difficult to assess globally. The brain is a highly interconnected organ, with interdependence mediated not only by neuronal connections, but also by means of cellular migration, common vascular supply, physical constraints, or other factors. As a result, radiation damage to one brain region has the potential to perturb brain development more broadly. A systematic study of such relationships is lacking—and infeasible in humans—but would have important implications for RT planning and potential for understanding long-term effects on brain development.

The mouse brain provides a controlled experimental model in which the effects of radiation on brain development can be investigated in the absence of cancer and other treatment effects. After whole-brain irradiation in infancy, mice exhibit volume changes throughout much of the brain, with particularly prominent volume and growth decreases in the olfactory bulbs (OBs) and connecting WM, the anterior commissure (AC).[17–19] In this paper, we investigated the dependence of radiation-induced volume change over the whole brain on the spatial distribution of delivered dose. We quantified volume changes within irradiated and unirradiated brain regions. We focused our investigation on the pars anterior of the AC, OBs, and lateral ventricles (LVs), whose lateral walls contain the neurogenic subventricular zone (SVZ). These structures are sufficiently separated spatially that each can be targeted individually with minimal delivered dose to the others.

Furthermore, the AC, OB, and SVZ regions represent different tissue types, separating WM, neuronal, and neurogenic tissues, respectively. The OBs are connected to one another through the WM of the AC, via the anterior olfactory nucleus (AON), and further connect to central brain regions such as the hypothalamic and amygdaloid via the lateral olfactory tract (LOT).[20,21] The OBs also depend on SVZ neurogenesis for neuroblasts to replenish neuronal populations,[22] such that impaired SVZ neurogenesis results in reduced OB neuronal populations and impaired olfactory memory formation.[23,24] Likewise, decreased olfactory function results in reduced SVZ neurogenesis.[25] The interdependence and spatial separation of the AC-OB-LV regions of interest (ROIs) provide the opportunity to investigate the developmental repercussions of focal radiation damage to these different tissue types.

We evaluated brain structure volumes in early adulthood after radiation treatment of the whole brain or of the AC, OB, or LV ROIs in infancy. We initially hypothesized that, by adulthood, large volume changes would be present in the AC after AC irradiation, while disruption of SVZ neurogenesis would account for a significant proportion of OB volume change after LV irradiation. Our results refute parts of this hypothesis and highlight that off-target effects, here defined as radiation-induced volume changes in unirradiated brain structures, account for a significant component of radiation-induced volume change in the developing mouse brain.

Materials and Methods

Three separate groups of mice were prepared for the experiments in this study (shown graphically in Supplementary Figure S1). The first group of mice was perfusion fixed at postnatal day (P) 16 for 2 purposes: (i) generation of a combined MRI and micro(μ)-CT atlas for radiation treatment planning ($N = 6$) and (ii) film dosimetry to confirm delivered doses ($N = 3$ for each of 4 RT plans). The second group of mice ($N = 12$) was irradiated at P16 and then perfusion fixed 2 hours later in order to assess spatial distribution of deposited dose histologically using γ-H2AX as a marker of DNA double-strand breaks ($N = 3$ for each RT plan). For the final group, mice ($N = 72$) were irradiated at P16 with 1 of 4 RT plans (or sham treated) and then perfusion fixed at P63 (early

adulthood) for morphological assessment with ex vivo MRI. A subset were further processed for histological analysis of neurogenesis and myelin basic protein (MBP). All animal experiments were approved by the Ontario Cancer Institute or the Centre for Phenogenomics Animal Care Committees.

Treatment Planning

To facilitate treatment planning, 6 P16 mouse head specimens were used to generate a representative, co-registered μ-CT and MR image (see Supplementary Methods). Image Hounsfield Unit values for the μ-CT images were calibrated to mouse bone densities obtained from 2 mouse bone phantoms (Bruker). Average representations of the 6 μ-CT and MR images were generated independently by iterative registration of all images to generate an unbiased average (as described below). A segmented neuroanatomical MRI atlas was registered to the average P16 MR image, which was in turn affine registered to the average μ-CT image (Supplementary Figure S2). This resulted in a mapping of the segmented atlas into the space of the average μ-CT image and provided ROI definitions for treatment planning. Using a validated preclinical treatment planning software (SmART-Plan, Precision X-ray),[26,27] simple beam geometries with circular collimation were designed to deliver 8 Gy to each ROI (whole brain, AC, OB, and LV). Radiochromic film dosimetries in separate P16 head specimens were performed in order to quantify the dose deposited (Supplementary Figure S3).

Brain Irradiation Procedure

Mice were anesthetized using 5% isoflurane in an induction chamber and then maintained under 2% anesthesia during the irradiation procedure. Whole-brain and focal irradiation (225 kV, 13 mA, 0.3 mm Cu filtration) was delivered at P16 via the XRAD-225Cx system (Precision X-ray) using 15 mm (whole-brain irradiation [WB-Irr], $N = 9$), 2.5 mm (AC irradiation [AC-Irr], $N = 12$), 5 mm (OB irradiation [OB-Irr], $N = 14$), and 2.5 mm (LV irradiation [LV-Irr], $N = 9$) circular collimators. Assuming an α/β of ~2 Gy for brain tissue, 8 Gy represents a biologic equivalent dose of 20 Gy in 2 Gy daily fractions,[28] consistent with RT doses used for acute lymphoblastic leukemia (though slightly lower than typical brain tumor treatments). In past work, we have shown that this dose results in volume differences in the brain consistent with human observations.[17,19] A frame with bite and ear bars (for dorsoventral beam plans) or a molded platform (for mediolateral beam plans) was used to stabilize the mouse and cranium during irradiations. Sham treatments for control subjects included handling and isoflurane anesthesia for 20 min, equivalent to the duration of an average radiation treatment. To position the mice initially and to check for any movement, in vivo cone-beam CT scans at a 200 μm isotropic resolution were acquired before and after dose delivery (100 kV, 100 μA, 2 mm Al filtration) with imaging doses ≤1 cGy.[29] To align the mouse and radiation treatment plans, the pre-irradiation CT volume was rigidly registered to the P16 μ-CT atlas on which planning had been performed using the Pilot software of the XRAD-225Cx micro-irradiator.[29]

Ex Vivo MRI

After irradiation, mice were housed in standard cages until P63 (young adult) and then prepared for ex vivo MRI as previously described.[30,31] The cohort of P16 mice required for treatment planning atlas were prepared identically. Ex vivo MRI was performed using a 3-D fast spin echo pulse sequence[32] (40 μm isotropic resolution, repetition time = 350 ms, effective echo time = 30 ms, echo spacing = 12 ms, echo train length = 6, scan time = 14 h, matrix size = 504 × 504 × 630).

Volume Analysis

An automated, registration-based image analysis pipeline was used to quantify brain structure differences between control and irradiated cohorts and to generate average images for the P16 treatment planning atlas.[33] In each case, all images were transformed to a consensus average space through a process of iterative registrations.[34] Average images were generated by voxel-by-voxel averaging of component images in the average space. Volume change at each voxel was computed from the vector deformations mapping individuals to the average, and then compared between treatment cohorts. Voxel volumes were then fit with a linear model. In addition, a segmented neuroanatomical atlas was registered to the consensus average space and the volume of defined structures was computed for each image.[35] Comparisons of structure volume between groups was achieved by a pairwise t-test. Multiple comparisons were corrected using the false discovery rate and thresholds set using q-values.

Histology, Cell Counting, and MBP Staining Analysis

To assess the spatial distribution of radiation delivered for each ROI, a group of mice was irradiated and then perfusion-fixed 2 h later for γ-H2AX staining. Samples were prepared in paraffin blocks at the STTARR Innovation Centre (see Supplementary Methods). For histological analyses of myelination and neurogenesis in P63 samples after irradiation at infancy, mouse brains were dissected and cryopreserved before being cut into 40-μm-thick sections. Counting of doublecortin (DCX)-positive cells was performed within the dentate gyrus (DG) as previously described,[36] with the observer blinded to the treatment. For comparisons between groups, the average number of target cells was computed across at least 3 animals. A nonstereologic method was used to estimate the cell numbers in the SVZ, AC, and corpus callosum (CC). Complete counts of MBP+ cells in the AC and CC were obtained in 3 sections per mouse, where cells with MBP staining around nuclei stained with 4′,6′-diamidino-2-phenylindole (DAPI) were considered MBP+. For semiquantitative analysis of MBP fluorescence intensity, the AC and CC were contoured, and histograms from the ROI in the red channel were used to analyze staining intensity (arbitrary units) using Photoshop after subtracting background signal measured from the ventricle.[37] The MBP staining intensity for each animal represented the mean staining intensity of at least 2 sections

per region per mouse. Analysis of DCX+ cells and MBP staining intensity was performed using one-way ANOVA with Tukey's correction.

Results

Image-Guided RT Can Be Used to Target Substructures of the P16 Mouse Brain

Simulated treatment plans were generated to deliver an average ROI dose of 8 ± 0.4 Gy for all cohorts (Fig. 1A). Beam center placement in the AC-Irr plan was slightly ventral and rostral to the AC so as to target the pars anterior of the AC while avoiding the SVZ neurogenic niche. Verification of spatial dose distribution for all cohorts was performed by mapping DNA double-strand breaks marked by the phosphorylated histone protein variant, γ-H2AX (Fig. 1B). Dose was quantified using radiochromic film dosimetry by irradiating films placed perpendicular to beam orientation inside brain tissue of ex vivo mouse heads, and yielded mean doses of 7.8 ± 0.2 Gy, 7.5 ± 0.1 Gy, 7.8 ± 0.2 Gy, and 8.1 ± 0.1 Gy for WB-Irr, AC-Irr, OB-Irr, and LV-Irr, respectively (Supplementary Figure S3). No changes in home cage behavior were observed in any of the radiation or sham-treated mice.

Significant Off-Target Volume Changes Accompany Radiation Damage in Targeted Brain Regions

Radiation at P16 resulted in significant volume changes at P63, with notable differences between treatment groups.
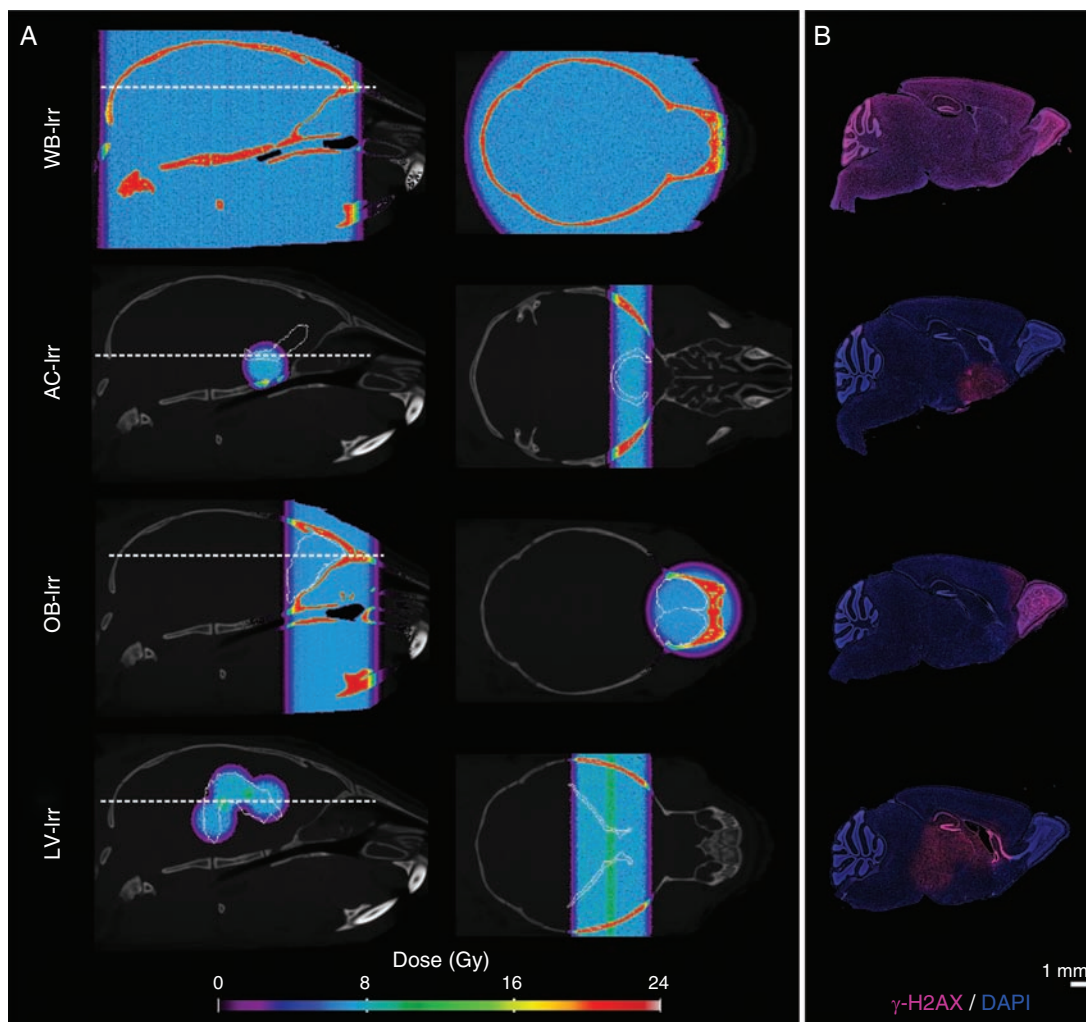

Fig. 1   Planned dose distributions and biological verification of targeting in whole-brain (WB-Irr) and focal irradiation cohorts (AC-, OB-, and LV-Irr). (A) Dose distributions are represented as a colormap overlaid on top of a grayscale image of the average P16 CT image. Cyan colors represent a dose of ~8 Gy. The first and second columns indicate sagittal and axial views, respectively, with the ROI from the registered atlas outlined in white. (B) Representative sagittal sections of P16 mouse brains collected 2 h post-irradiation and stained with γ-H2AX (magenta) show the spatial distribution achieved in vivo (*n* = 3 mice per cohort). DAPI counterstain is shown in blue to indicate nuclei.

Results are represented voxel-wise in Fig. 2. WB-Irr mice showed widespread volume reductions characteristic of previous work ($q < 0.05$),[14] including in the OBs, hippocampus, AC, CC, and several other prominent WM structures. An increased volume was detected in the rostral region of the striatum. Surprisingly, targeting of the AC (AC-Irr) resulted in negligible volume change at P63. Notably absent was any detectable change in the AC itself. OB targeting (OB-Irr) significantly impacted OB development and further resulted in volume change in the AC and isolated regions of the CC and parietal cortex. Irradiation of the SVZ neurogenic niche in the LV-Irr group yielded a volume reduction in the area targeted, including localized regions of the CC and hippocampus, and produced off-target effects in the OBs and the AC.

Volume differences between groups were further summarized by quantifying structure volume using an atlas of 182 structures. Results focused on the AC-OB-LV system are presented in Fig. 3. Brain-wide results are provided in Supplementary Figure S5. As expected, the largest volume

differences were present in the WB-Irr group. The magnitude of volume changes in targeted and off-target regions in the focal irradiation groups provides a measure of the relative importance of these effects in the brain's response to radiation. The volume of the AC was reduced by ~19% in the WB-Irr group. The total volume of the AC was not significantly different from controls after targeting of the AC, but its volume was reduced by ~8% ($q < 0.01$) and ~5% ($q < 0.05$) after irradiation of the OBs and LVs, respectively (Fig. 3A). The total volume of the OBs was ~17% smaller in WB-Irr mice relative to controls ($q < 0.01$). No OB volume change was present in the AC-Irr group, but direct OB targeting (OB-Irr) resulted in ~7% volume loss ($q < 0.01$; Fig. 3B), and targeting of the SVZ neurogenic niche (LV-Irr) resulted in ~6% loss ($q < 0.01$). Segmentation of the layers of the OB to localize the volumetric differences showed that both OB-Irr and LV-Irr mice displayed similar volumetric reductions in all 5 main OB layers ranging from the innermost granule cell layer (GCL) to the outermost glomerular layer (GL) (Fig. 3C, D). The volume of the LOT
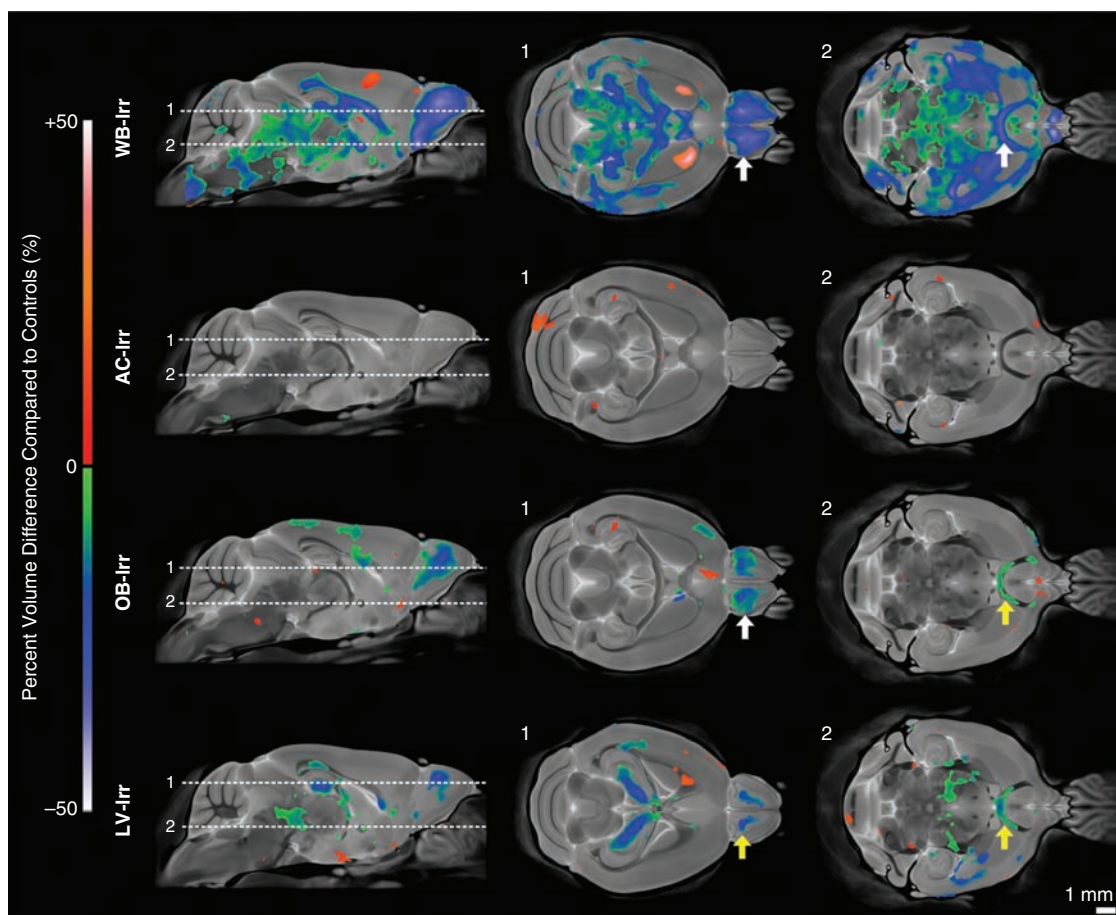
Fig. 2 Voxel-wise comparison of significant volume differences of adult mice (P63) after whole-brain or focal irradiation at infancy (P16) ($q < 0.05$). The first column shows mid-sagittal views of the average adult mouse brain with a colormap overlay showing significant percent volume differences of irradiated mice compared with controls. The second and third columns show the indicated axial views. White and yellow arrows indicate direct and off-target effects of radiation damage, respectively.
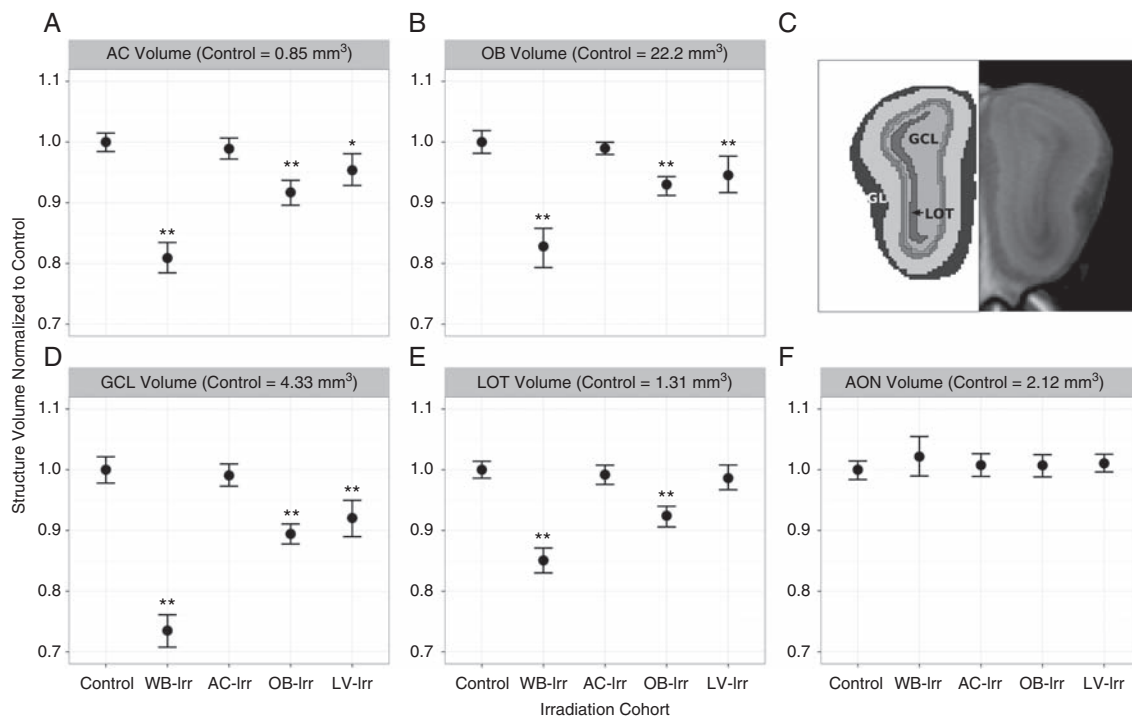
Fig. 3 Structure-wise comparison of volume differences after whole-brain versus focal irradiation. Normalized brain structure volumes of the (A) AC, (B) OBs, (D) GCL of the OBs, (E) LOT, and (F) AON of the OBs are displayed for all irradiation cohorts. (C) The location of the innermost GCL, the LOT, and the outermost GL are highlighted in a coronal view of the OBs. Error bars represent 95% confidence intervals; *$q < 0.05$ and **$q < 0.01$ relative to controls.

was reduced in WB-Irr and OB-Irr mice (Fig. 3E). The AON displayed no significant volumetric differences even after WB-Irr (Fig. 3F).

Off-target volume reductions were also present in other brain regions (Fig. 4). The volume of the pars posterior of the AC (quantified separately from the pars anterior) was decreased by ~23% in the WB-Irr cohort, but also showed volume decreases of ~8% in the LV-Irr group (Fig. 4B). The CC exhibited an overall volume decrease of ~12% in the WB-Irr group, but also showed decreases of ~3% and ~5% in the OB-Irr and LV-Irr groups, respectively (Fig. 4D). The parietal cortex showed a significant volume change in the OB-Irr group ($q < 0.05$; Fig. 4C), but not in any of the other treatment groups (despite receiving radiation in both the WB-Irr and LV-Irr groups).

Off-Target Effects Impact Neurogenesis but Show Limited Effects on Myelination

We evaluated myelination using immunohistochemistry for MBP. Loss of MBP staining intensity was observed after WB-Irr (Fig. 5). However, no significant differences in MBP staining intensity in the AC or CC were observed in the focal RT groups compared with controls. We also did not observe any significant change in the number of MBP+ cells per cubic millimeter in the AC or CC in any of the irradiated groups compared with controls (data not shown).

Loss of cells immunoreactive for DCX, a marker for neuroblasts, was apparent in the SVZ of all radiation-treated mice (Fig. 6A, C), although the AC-Irr group retained more DCX+ cells than the WB-Irr group. Neurogenesis was also quantified in the DG (Fig. 6B, D) within the subgranular zone (a neurogenic niche distinct from the SVZ); the largest loss of DCX+ cells occurred in WB-Irr mice. A greater number of DCX+ cells were retained in all focal treatment groups, including the LV-Irr group, in which the DG received a substantial radiation dose. DCX+ cells in the DG were also decreased in the OB-Irr group, although no part of the DG was targeted in this group.

Discussion

Children who receive RT as part of cancer treatment routinely exhibit structural changes in the brain thought to be linked to cognitive late effects.[5,38,39] The interaction between and relative significance of direct radiation damage and off-target effects are important for understanding the genesis of these structural changes. This study evaluated the effects of radiation damage in 3 ROIs with different tissue/cell types and evaluated the resulting alterations to brain structure. To the best of our knowledge, this is the first study to quantify the contribution of localized radiation
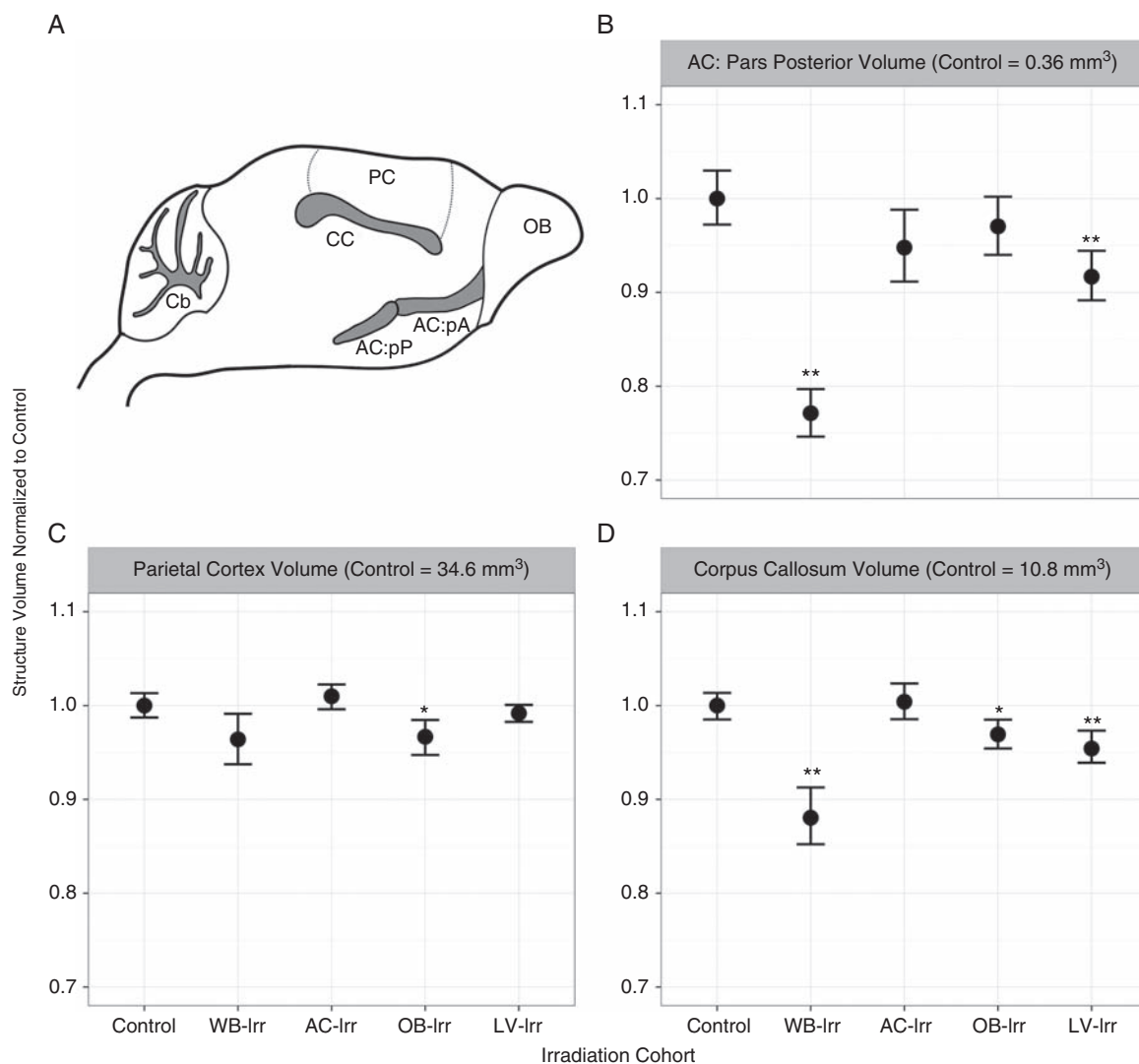
Fig. 4 Volume differences in central and cortical brain structures after whole-brain and focal irradiations. (A) The location of the AC: pars posterior (AC:pP), parietal cortex (PC), and corpus callosum (CC) in relation to the OBs and cerebellum (Cb) are shown in a mouse brain schematic. (B–D) Brain structure volumes of the AC: pars posterior (B), parietal cortex (C), and corpus callosum (D) for all cohorts are shown. Error bars represent 95% confidence intervals; *$q < 0.05$ and **$q < 0.01$ relative to controls.

damage to WM, neuronal, and neurogenic regions on subsequent brain development as a whole.

One of the unexpected findings in this study is the response of WM in the AC after radiation. WM regions exhibit greater volume loss after RT in patients than do gray matter regions, and hence are often considered more radiosensitive.[40] However, WM in the AC showed no significant volume or MBP staining intensity change after being directly targeted with radiation. On the contrary, a smaller AC volume was observed after irradiation of the OB or LV ROIs. Interestingly, a similar off-target volume effect was noted in the CC, which was smaller after irradiation of the OB. These observations challenge the idea that WM is more radiosensitive than gray matter and suggest that volume loss in WM includes significant off-target effects due to radiation

damage in other brain regions. Several mechanisms are likely involved in generating off-target effects in the WM. Given the reduction of AC and LOT volumes after OB-Irr (but not after AC-Irr; Figure 3A, E), and the location of the LOT and AC somata,[20,21,41] one may speculate that irradiation of neuronal cell bodies results in cellular damage or apoptosis that leads to downstream Wallerian-like axon degeneration, inducing secondary consequences within the WM. While appealing, this explanation does not account for all WM results, since volume changes in the AC were also apparent in the LV-Irr group, in which the neuronal cell bodies should be largely spared, thus indicating additional contributing factors possibly related to precursor cells in the SVZ. Moreover, although there was significant volume loss in the AC in the OB-Irr and LV-Irr groups, changes in MBP
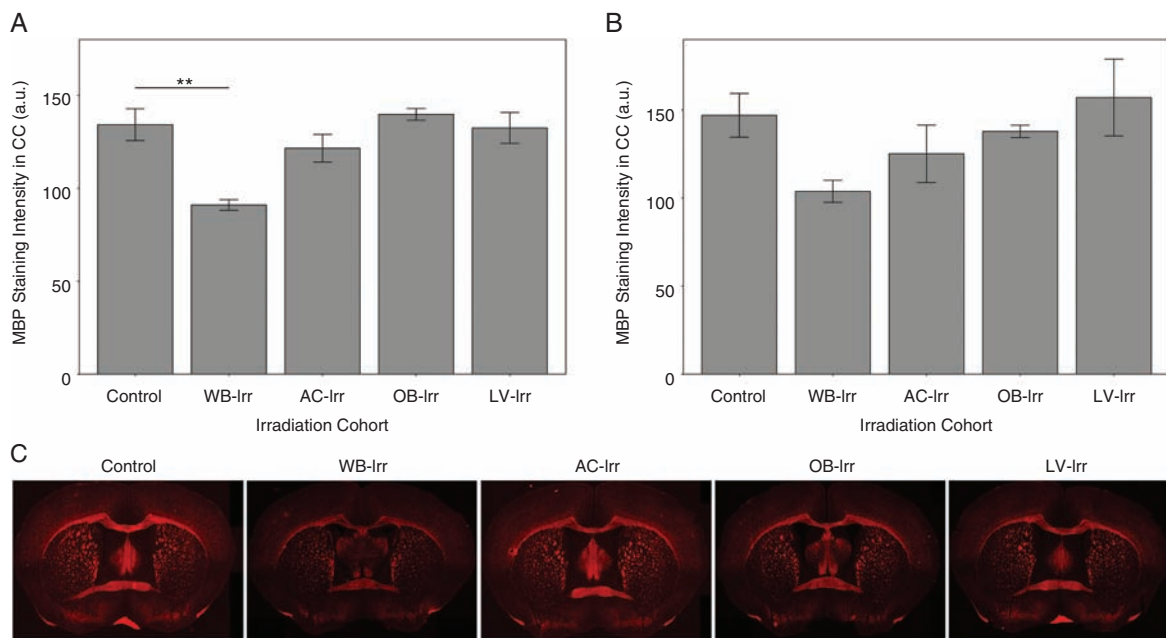
Fig. 5 MBP staining intensity in P63 brains irradiated at infancy with whole-brain or focal irradiation. Quantification of MBP staining intensity for all irradiation cohorts is shown for the CC (A) and the AC (B). (C) Representative coronal sections are provided showing the AC and CC ($n = 3$ mice per cohort). Error bars indicate standard error of the mean. **$q < 0.01$ after one-way ANOVA with Tukey's post-hoc test.

staining intensity were not detected. Decreased CC MBP staining intensity was observed in the WB-Irr group, indicating that broader targeting does result in significant myelination changes, but was not present in the LV-Irr group, even though the CC received some radiation. Although our experiments did not explicitly target regions around the CC, these observations may indicate that myelination changes in this model, like WM volume changes, have off-target contributions. Further experiments are warranted elucidating the contribution of axonal degeneration, stem cell depletion, and inflammation on the off-target WM changes observed after RT.

Previous work has shown that SVZ irradiation affects neurogenesis in the stem cell niche and neuroblast migration along the rostral migratory path.[42] Our results are consistent with these observations, showing volumetric deficits in the OB after irradiation of the SVZ and surrounding area (LV-Irr group). Interestingly, irradiation of the OBs (OB-Irr) and AC (AC-Irr) also resulted in a significant reduction in neuroblasts in the SVZ (Fig. 6C), even though the latter resulted in no significant volume changes. This indicates that radiation damage in other brain regions affects stem cells in the SVZ. Indeed, under appropriate circumstances, the SVZ niche has been shown to supply cells to WM regions in the striatum, fimbria, fornix, and CC.[42] In these cases, SVZ-derived cells can adopt an oligodendroglial rather than neuronal fate, providing oligodendrocyte progenitor cells and oligodendrocytes.[43] Given that SVZ stem cells may respond and promote recovery and repair after ischemia[44] and neurodegenerative disease,[45] the response of these cells to whole-brain and focal irradiation merits

further investigation. Although the presence and role of SVZ neurogenesis in humans is debated,[46–48] efforts to protect neurogenic niches in patients receiving cranial RT could have important implications due to off-target effects.[49–51]

It is unlikely that scattered dose contributed significantly to the findings in this paper. We have previously shown that whole-brain radiation doses up to 3 Gy resulted in only small volume changes through development.[19] Our dose maps suggest that scattered dose to the AC was limited to ~1 Gy in the LV-Irr group and that the SVZ received a negligible dose in the AC-Irr group (Supplementary Figure S4A). Moreover, targeting of the AC with ~8 Gy produced negligible volume change, so it seems unlikely that a much smaller scattered dose could do so. As a metric, neurogenesis is likely to be more sensitive to low dose RT than volume change, but the changes in neurogenesis did not track clearly with scatter doses. For these reasons, off-target effects resulting from the interaction of brain development and focal radiation provide a more plausible explanation of our observations.

In this study, we investigated volume changes in the whole brain after focally targeting WM (AC), neuronal (OBs), and neurogenic (LVs) regions with radiation. Volume and histological results emphasize that both direct targeting and off-target effects have important consequences for brain development. WM in the AC showed no significant volume change after direct targeting but exhibited significant losses after targeting of the OBs or LVs. Similarly, histological analyses revealed that off-target effects impact SVZ neurogenesis. Although the extent to which observations in the mouse model apply to childhood brain tumor patients will need to be established, the substantial
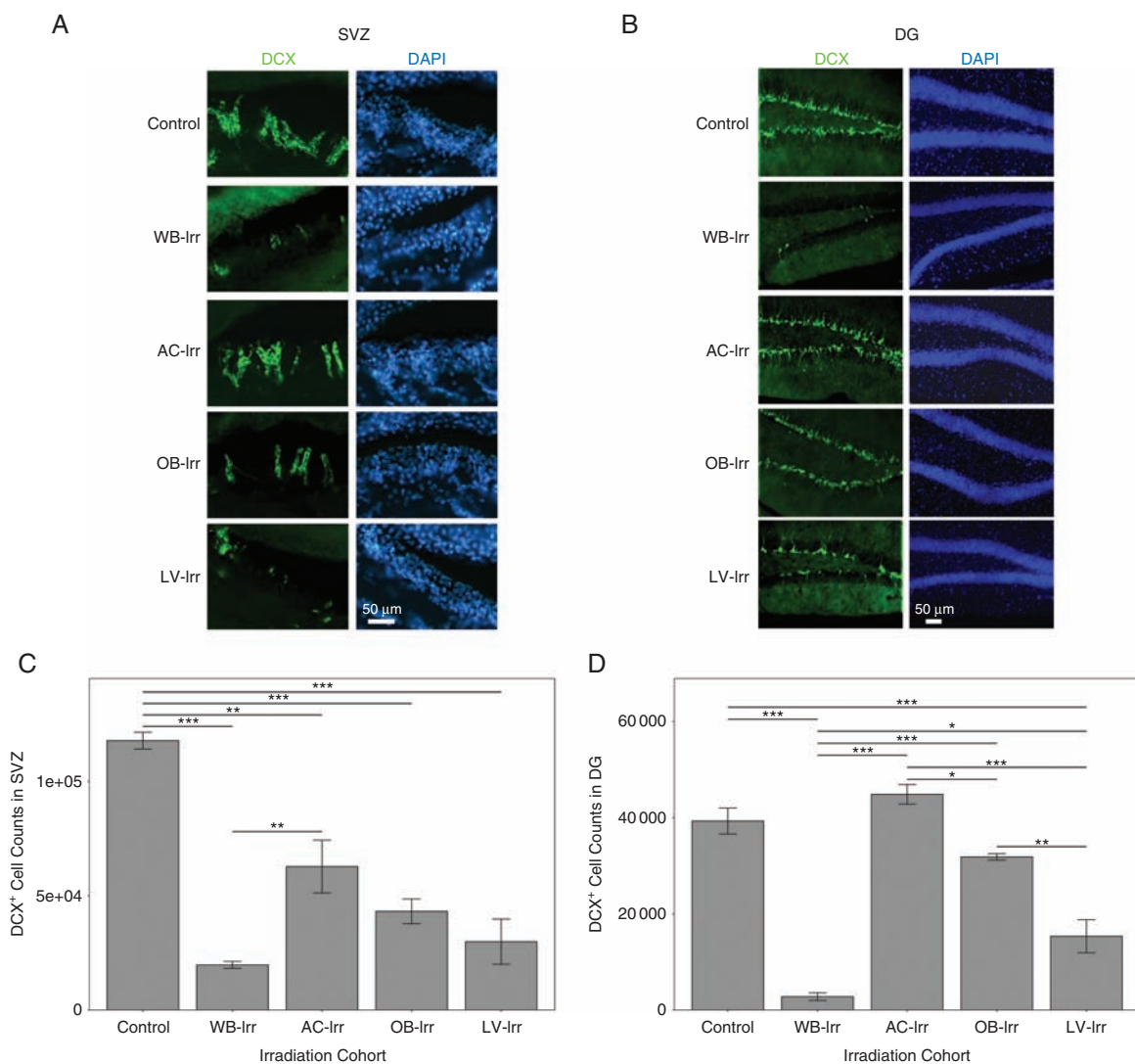
Fig. 6   The developmental impact of whole-brain and focal irradiations on neurogenesis in the SVZ and DG. Representative coronal sections of the SVZ (A) and the DG (B) in P63 mouse brains irradiated at infancy and stained for DCX (green; left column) ($n = 3$ mice per cohort). DAPI counterstain is shown in blue (right column). Quantification of DCX+ cell number is shown for the SVZ (C) and DG (D). Error bars indicate standard error of the mean. *$q < 0.05$, **$q < 0.01$, ***$q < 0.001$ after one-way ANOVA corrected with Tukey's multiple comparisons test.

contribution of off-target effects within the brain after RT may have important implications. For example, emerging region-sparing strategies intended to reduce cognitive impairments using reduced-dose intensity-modulated RT, arc therapy, or even strategic shielding with collimators may benefit by considering off-target effects at the dose planning stage; dose reduction to regions of neurogenesis or regions of WM may not produce the benefits expected owing to off-target effects coming from other irradiated structures. It may be possible to exploit dose gradients across different tumor types to explore this in treated patients. In mice, elucidation of the biological mechanism underlying off-target effects within the brain and investigation of the strength of the anatomy-behavior correlation in this context would be of significant interest.

Supplementary Material

Supplementary material is available at *Neuro-Oncology* online.

Funding

Conflict of interest: D.A.J. is listed as an inventor of the irradiator used herein, which is licensed to Precision X-Ray Inc for commercial development.

References

1. Koeller KK, Rushing EJ. From the archives of the AFIP: medulloblastoma: a comprehensive review with radiologic-pathologic correlation. *Radiographics*. 2003;23(6):1613–1637.

2. Moore BD 3rd. Neurocognitive outcomes in survivors of childhood cancer. *J Pediatr Psychol*. 2005;30(1):51–63.

3. Dennis M, Spiegler BJ, Hetherington CR, Greenberg ML. Neuropsychological sequelae of the treatment of children with medulloblastoma. *J Neurooncol*. 1996;29(1):91–101.

4. Armstrong GT, Liu Q, Yasui Y, et al. Long-term outcomes among adult survivors of childhood central nervous system malignancies in the Childhood Cancer Survivor Study. *J Natl Cancer Inst*. 2009;101(13):946–958.

5. Reddick WE, Glass JO, Palmer SL, et al. Atypical white matter volume development in children following craniospinal irradiation. *Neuro Oncol*. 2005;7(1):12–19.

6. Palmer SL, Reddick WE, Glass JO, Gajjar A, Goloubeva O, Mulhern RK. Decline in corpus callosum volume among pediatric patients with medulloblastoma: longitudinal MR imaging study. *AJNR Am J Neuroradiol*. 2002;23(7):1088–1094.

7. Parihar VK, Limoli CL. Cranial irradiation compromises neuronal architecture in the hippocampus. *Proc Natl Acad Sci U S A*. 2013;110(31):12822–12827.

8. Atkinson S, Li YQ, Wong CS. Changes in oligodendrocytes and myelin gene expression after radiation in the rodent spinal cord. *Int J Radiat Oncol Biol Phys*. 2003;57(4):1093–1100.

9. Panagiotakos G, Alshamy G, Chan B, et al. Long-term impact of radiation on the stem cell and oligodendrocyte precursors in the brain. *PLoS One*. 2007;2(7):e588.

10. Monje ML, Mizumatsu S, Fike JR, Palmer TD. Irradiation induces neural precursor-cell dysfunction. *Nat Med*. 2002;8(9):955–962.

11. Chow BM, Li YQ, Wong CS. Radiation-induced apoptosis in the adult central nervous system is p53-dependent. *Cell Death Differ*. 2000;7(8):712–720.

12. Boström M, Kalm M, Karlsson N, Hellström Erkenstam N, Blomgren K. Irradiation to the young mouse brain caused long-term, progressive depletion of neurogenesis but did not disrupt the neurovascular niche. *J Cereb Blood Flow Metab*. 2013;33(6):935–943.

13. Maier DM, Landauer MR. Effects of acute sublethal gamma radiation exposure on aggressive behavior in male mice: a dose-response study. *Aviat Space Environ Med*. 1989;60(8):774–778.

14. Rao AA, Ye H, Decker PA, Howe CL, Wetmore C. Therapeutic doses of cranial irradiation induce hippocampus-dependent cognitive deficits in young mice. *J Neurooncol*. 2011;105(2):191–198.

15. Roughton K, Kalm M, Blomgren K. Sex-dependent differences in behavior and hippocampal neurogenesis after irradiation to the young mouse brain. *Eur J Neurosci*. 2012;36(6):2763–2772.

16. Belarbi K, Jopson T, Arellano C, Fike JR, Rosi S. CCR2 deficiency prevents neuronal dysfunction and cognitive impairments induced by cranial irradiation. *Cancer Res*. 2013;73(3):1201–1210.

17. Nieman BJ, de Guzman AE, Gazdzinski LM, et al. White and gray matter abnormalities after cranial radiation in children and mice. *Int J Radiat Oncol Biol Phys*. 2015;93(4):882–891.

18. Gazdzinski LM, Cormier K, Lu FG, Lerch JP, Wong CS, Nieman BJ. Radiation-induced alterations in mouse brain development characterized by magnetic resonance imaging. *Int J Radiat Oncol Biol Phys*. 2012;84(5):e631–e638.

19. de Guzman AE, Gazdzinski LM, Alsop RJ, et al. Treatment age, dose and sex determine neuroanatomical outcome in irradiated juvenile mice. *Radiat Res*. 2015;183(5):541–549.

20. Shipley MT, Adamek GD. The connections of the mouse olfactory bulb: a study using orthograde and retrograde transport of wheat germ agglutinin conjugated to horseradish peroxidase. *Brain Res Bull*. 1984;12(6):669–688.

21. Walz A, Omura M, Mombaerts P. Development and topography of the lateral olfactory tract in the mouse: imaging by genetically encoded and injected fluorescent markers. *J Neurobiol*. 2006;66(8):835–846.

22. Doetsch F, Alvarez-Buylla A. Network of tangential pathways for neuronal migration in adult mammalian brain. *Proc Natl Acad Sci U S A*. 1996;93(25):14895–14900.

23. Lazarini F, Mouthon MA, Gheusi G, et al. Cellular and behavioral effects of cranial irradiation of the subventricular zone in adult mice. *PLoS One*. 2009;4(9):e7017.

24. Valley MT, Mullen TR, Schultz LC, Sagdullaev BT, Firestein S. Ablation of mouse adult neurogenesis alters olfactory bulb structure and olfactory fear conditioning. *Front Neurosci*. 2009;3:51.

25. Xu Z, Gao Y, Xu F. Deficits of peripheral olfactory inputs reduce cell proliferation in the adult subventricular and subgranular zones. *Neurosci Lett*. 2013;541:269–274.

26. Granton PV, Podesta M, Landry G, Nijsten S, Bootsma G, Verhaegen F. A combined dose calculation and verification method for a small animal precision irradiator based on onboard imaging. *Med Phys*. 2012;39(7):4155–4166.

27. van Hoof SJ, Granton PV, Verhaegen F. Development and validation of a treatment planning system for small animal radiotherapy: SmART-Plan. *Radiother Oncol*. 2013;109(3):361–366.

28. Fowler JF. The linear-quadratic formula and progress in fractionated radiotherapy. *Br J Radiol*. 1989;62(740):679–694.

29. Clarkson R, Lindsay PE, Ansell S, et al. Characterization of image quality and image-guidance performance of a preclinical microirradiator. *Med Phys*. 2011;38(2):845–856.

30. Cahill LS, Laliberté CL, Ellegood J, et al. Preparation of fixed mouse brains for MRI. *Neuroimage*. 2012;60(2):933–939.

31. de Guzman AE, Wong MD, Gleave JA, Nieman BJ. Variations in postperfusion immersion fixation and storage alter MRI measurements of mouse brain morphometry. *Neuroimage*. 2016;142:687–695.

32. Spencer Noakes TL, Henkelman RM, Nieman BJ. Partitioning k-space for cylindrical three-dimensional rapid acquisition with relaxation enhancement imaging in the mouse brain. *NMR Biomed*. 2017;30(11):doi: 10.1002/nbm.3802.

33. Lerch JP, Sled JG, Henkelman RM. MRI phenotyping of genetically altered mice. *Methods Mol Biol*. 2011;711:349–361.

34. Avants BB, Epstein CL, Grossman M, Gee JC. Symmetric diffeomorphic image registration with cross-correlation: evaluating automated labeling of elderly and neurodegenerative brain. *Med Image Anal*. 2008;12(1):26–41.

35. Dorr AE, Lerch JP, Spring S, Kabani N, Henkelman RM. High resolution three-dimensional brain atlas using an average magnetic resonance image of 40 adult C57Bl/6J mice. *Neuroimage*. 2008;42(1):60–69.

36. Lu F, Li YQ, Aubert I, Wong CS. Endothelial cells regulate p53-dependent apoptosis of neural progenitors after irradiation. *Cell Death Dis*. 2012;3:e324.

37. Agley CC, Velloso CP, Lazarus NR, Harridge SD. An image analysis method for the precise selection and quantitation of fluorescently labeled cellular constituents: application to the measurement of human muscle cells in culture. *J Histochem Cytochem*. 2012;60(6):428–438.

38. Riggs L, Bouffet E, Laughlin S, et al. Changes to memory structures in children treated for posterior fossa tumors. *J Int Neuropsychol Soc*. 2014;20(2):168–180.

39. Nagel BJ, Palmer SL, Reddick WE, et al. Abnormal hippocampal development in children with medulloblastoma treated with risk-adapted irradiation. *AJNR Am J Neuroradiol*. 2004;25(9):1575–1582.

40. Moxon-Emre I, Bouffet E, Taylor MD, et al. Vulnerability of white matter to insult during childhood: evidence from patients treated for medulloblastoma. *J Neurosurg Pediatr*. 2016;18(1):29–40.

41. Reyher CK, Schwerdtfeger WK, Baumgarten HG. Interbulbar axonal collateralization and morphology of anterior olfactory nucleus neurons in the rat. *Brain Res Bull*. 1988;20(5):549–566.

42. Achanta P, Capilla-Gonzalez V, Purger D, et al. Subventricular zone localized irradiation affects the generation of proliferating neural precursor cells and the migration of neuroblasts. *Stem Cells*. 2012;30(11):2548–2560.

43. Menn B, Garcia-Verdugo JM, Yaschine C, Gonzalez-Perez O, Rowitch D, Alvarez-Buylla A. Origin of oligodendrocytes in the subventricular zone of the adult brain. *J Neurosci*. 2006;26(30):7907–7918.

44. Macas J, Nern C, Plate KH, Momma S. Increased generation of neuronal progenitors after ischemic injury in the aged adult human forebrain. *J Neurosci*. 2006;26(50):13114–13119.

45. Ernst A, Alkass K, Bernard S, et al. Neurogenesis in the striatum of the adult human brain. *Cell*. 2014;156(5):1072–1083.

46. Sanai N, Tramontin AD, Quiñones-Hinojosa A, et al. Unique astrocyte ribbon in adult human brain contains neural stem cells but lacks chain migration. *Nature*. 2004;427(6976):740–744.

47. Sanai N, Nguyen T, Ihrie RA, et al. Corridors of migrating neurons in the human brain and their decline during infancy. *Nature*. 2011;478(7369):382–386.

48. Wang C, Liu F, Liu YY, et al. Identification and characterization of neuroblasts in the subventricular zone and rostral migratory stream of the adult human brain. *Cell Res*. 2011;21(11):1534–1550.

49. Blomstrand M, Brodin NP, Munck Af Rosenschöld P, et al. Estimated clinical benefit of protecting neurogenesis in the developing brain during radiation therapy for pediatric medulloblastoma. *Neuro Oncol*. 2012;14(7):882–889.

50. Oehler J, Brachwitz T, Wendt TG, Banz N, Walther M, Wiezorek T. Neural stem cell sparing by linac based intensity modulated stereotactic radiotherapy in intracranial tumors. *Radiat Oncol*. 2013;8:187.

51. Gondi V, Pugh SL, Tome WA, et al. Preservation of memory with conformal avoidance of the hippocampal neural stem-cell compartment during whole-brain radiotherapy for brain metastases (RTOG 0933): a phase II multi-institutional trial. *J Clin Oncol*. 2014;32(34):3810–3816.